Random walks with thermalizing collisions in bounded regions: Physical applications valid from the ballistic to diffusive regimes

C. M. Swank,[1] A. K. Petukhov,[2] and R. Golub[3]
[1]*Division of Physics, Math and Astronomy, California Institute of Technology, Pasadena, California 91125, USA*
[2]*Institut Laue-Langevin, BP156, 38042 Grenoble Cedex 9, France*
[3]*Physics Department, North Carolina State University, Raleigh, North Carolina 27695, USA*
(Received 31 March 2016; published 8 June 2016)

The behavior of a spin undergoing Larmor precession in the presence of fluctuating fields is of interest to workers in many fields. The fluctuating fields cause frequency shifts and relaxation which are related to their power spectrum, which can be determined by taking the Fourier transform of the auto-correlation functions of the field fluctuations. Recently we have shown how to calculate these correlation functions for all values of mean-free path (ballistic to diffusive motion) in finite bounded regions by using the model of persistent continuous time random walks (CTRW) for particles subject to scattering by fixed (frozen) scattering centers so that the speed of the moving particles is not changed by the collisions. In this work we show how scattering with energy exchange from an ensemble of scatterers in thermal equilibrium can be incorporated into the CTRW. We present results for 1, 2, and 3 dimensions. The results agree for all these cases contrary to the previously studied "frozen" models. Our results for the velocity autocorrelation function show a long-time tail ($\sim t^{-1/2}$), which we also obtain from conventional diffusion theory, with the same power, independent of dimensionality. Our results are valid for any Markovian scattering kernel as well as for any kernel based on a scattering cross section $\sim 1/v$.

DOI: 10.1103/PhysRevA.93.062703

I. INTRODUCTION

The dynamics of a system of spins moving under the influence of static and time-varying magnetic fields is a subject of wide-ranging scientific and technical interest. Both randomly fluctuating fields produced by a thermal reservoir and fluctuations seen by particles undergoing stochastic trajectories in inhomogeneous fields have been the subject of intense study over many decades. It was Bloembergen, Purcell, and Pound [1] who first showed, by using physical arguments based on Fermi's golden rule, that the relaxation rate is determined by the power spectrum of the fluctuating fields evaluated at the Larmor frequency. In general, power spectra of fluctuating quantities are given by the Fourier transform of the autocorrelation of the fluctuating variable. A short history of the development of the field can be found in the introductions to Refs. [2,3].

One of the applications of these techniques is to the next-generation searches for a particle electric dipole moment (EDM), which require measurements of spin dynamics in uniform magnetic fields with nanohertz precision. Furthermore, searches for fundamental forces beyond the standard model require similar accuracy in the measurement of longitudinal and transverse relaxation (T_1 and T_2) expected to be produced by the hypothesized interaction. The desire for such accurate predictions inspires the search for models of particle trajectories in the case of particles moving in inhomogeneous fields.

Redfield [4], as elucidated by Slichter [5], and McGregor [6] have given formal derivations of the relation between relaxation and the autocorrelation functions of the fields, and the method was applied to a "false EDM" systematic error, effecting searches for time reversal and parity-violating nonzero particle electric dipole moments [7,8]. General methods for obtaining auto-correlation functions for fluctuations produced by particles diffusing in inhomogeneous fields with arbitrary spatial variation have been given by Refs. [9] and [10].

This work has been extended by Ref. [11] to the case of arbitrary field variation and all values of scattering mean-free path (from ballistic to diffusive motion) in restricted geometries. The method used was based on the persistent continuous time random walk model of Masoliver *et al.* [12], who solved a transport equation for the Laplace–Fourier transform of the conditional probability $P(\vec{r},t)$, which is the probability that a particle located at $\vec{r} = 0$ at $t = 0$ will be found at position $\vec{r}$ at time t (sometimes called a propagator) for the case of an infinite domain. The model assumed a collection of fixed scattering centers ("frozen" environment) so that the speed of the particles was unchanged by the scattering events and was valid for all values of the mean-free path. The authors of Ref. [11] applied the results of Masoliver *et al.* [12] to two- and three-dimensional (2D and 3D) regions bounded by rectangles by using the method of images and used the resulting conditional probabilities to calculate a number of spectra of autocorrelation functions relevant to relaxation and frequency shifts in a range of problems. See Ref. [3] for an overview of the relation between correlation functions of fluctuating fields and physical phenomena.

In Refs. [13,14] the authors used a similar method to derive the propagator, conditional probability for one dimension, in the presence of an external force; for example, gravity, in the asymptotic limit of small spatial and temporal frequencies.

In the present work we apply the technique of Swank *et al.* [11] to the case of Markovian scattering in which each collision completely rethermalizes the scattered particles. The method applies equally to the case when the total inelastic scattering cross section $\sim 1/v$, with v being the particle velocity. We find that the results differ somewhat from those obtained by averaging the results for the frozen environment over the velocity distribution of the scattered particles and that the results for one, two, and three dimensions are identical when averaged over a Maxwell distribution. Furthermore, we show that, for stochastic bounded motion, the velocity

autocorrelation functions have long-time tails proportional to $t^{-1/2}$, in all cases where diffusion theory is valid, in agreement with the one-dimensional treatment in Ref. [15]. Other studies have shown that in nonbounded systems long-range hydrodynamic forces lead to different results ($\sim t^{-d/2}$) where d is the number of dimensions of the system. We present the results of applying our method to the physically interesting problems of the false EDM systematic error in searches for particle electric dipole moments and to calculating the position and velocity autocorrelation functions for particles confined to a bounded region, which determine frequency shifts and relaxation rates in NMR [3].

II. THE MODEL

A. Preliminaries: Persistent continuous time random walk in frozen environment

In this section we review the solution for the spectrum of the probability density of a persistent continuous time random walk (CTRW) as presented in the work of Weiss and co-workers [12]. The particles are assumed to travel ballistically with fixed velocity v between scattering events. The time between scattering events is governed by a distribution $\psi(t)$, such that the probability to scatter within a time segment dt is given by $\psi(t)dt$, and the probability to reach t without scattering is given by $\Psi(t) = \int_t^\infty \psi(t)dt$. The conditional probability $p(\mathbf{x},t)$, is calculated, as well as a scattering density $\rho(\mathbf{x},t)$, which is the probability of scattering at $\mathbf{x}$ and time t. A recursive equation that completely describes the CTRW is formed for the two densities,

$$\begin{aligned}\rho(\mathbf{x},t,v,\Omega) = {} & f(\mathbf{x},t,v)\alpha(\Omega)\psi(t) + \iiint d^3\mathbf{x}'dt'd\Omega' \\ & \times f(\mathbf{x}-\mathbf{x}',t-t',v)\beta(\Omega|\Omega')\psi(t-t') \\ & \times \int dv'\rho(\mathbf{x}',t',v'), \end{aligned} \tag{1}$$

$$\begin{aligned}p(\mathbf{x},t,v,\Omega) = {} & f(\mathbf{x},t,v)\alpha(\Omega)\Psi(t) + \iiint d^3\mathbf{x}'dt'd\Omega' \\ & \times f(\mathbf{x}-\mathbf{x}',t-t',v)\beta(\Omega|\Omega')\Psi(t-t') \\ & \times \int dv'\rho(\mathbf{x}',t',v'). \end{aligned} \tag{2}$$

In three dimensions the angular coordinates denoted by $\Omega = \{\theta,\phi\}$ has element $d\Omega = \sin\theta d\theta d\phi$. $\alpha(\Omega)$ is the initial angular density, while $\beta(\Omega|\Omega')$ is the conditional angular density having scattered from a previous angle Ω' and also known as the scattering kernel. We will assume the initial angular density to be isotropic and the angular conditional density to be isotropic and Markovian. Therefore, in three dimensions, we have,

$$\alpha(\Omega) = \beta(\Omega|\Omega') = \frac{1}{4\pi}.$$

In three dimensions $f(\mathbf{x},t,v)$ is given by

$$\begin{aligned}f(\mathbf{x},t,v) = {} & \delta(x - vt\sin\theta\cos\phi)\delta(y - vt\sin\theta\sin\phi) \\ & \times\delta(z - vt\cos\theta). \end{aligned} \tag{3}$$

The scattering time density will be assumed to follow a simple Poisson distribution:

$$\psi(t) = \frac{1}{\tau_c}e^{-\frac{t}{\tau_c}}, \tag{4}$$

where τ_c is the average collision time. The spectrum of the conditional density is found by applying the Laplace–Fourier transform to Eq. (2) [12]:

$$p(\mathbf{q},s) = \tau_c\frac{\arctan\left(\frac{qv\tau_c}{1+s\tau_c}\right)}{qv\tau_c - \arctan\left(\frac{qv\tau_c}{1+s\tau_c}\right)}. \tag{5}$$

In our previous work [11], we extended the free-space solution shown in Eq. (5) (for the 3D case) to the restricted domain in one, two, and three dimensions. In the present work we allow the velocity to change upon a scattering event, changing the model from a frozen model with fixed speed to one that allows momentum transfer. The approach is similar to that shown in Ref. [16]. We will see that the result differs from simply averaging the single velocity conditional density over velocity and that the results for three dimensions are identical to the results for lower dimensions, and a method for predicting three-dimensional results from a one-dimensional (1D) model (in Cartesian coordinates) is obtained. Results for the position and velocity autocorrelation functions and applications to the bounded domain are presented.

B. From the frozen environment to thermalization with momentum transfer

In the following we present our model of a CTRW with thermalization that we refer to as CTRWT. We start from the approach described above [12]. A change in velocity upon a gas scattering can be accounted for by including a probability distribution for the outgoing velocity after a scattering event. The treatment of v is identical to that of Ref. [12] for the angular density, except now we allow the vector velocity $\mathbf{v}$ to change. Therefore we extend functions $\alpha(\Omega)$ and $\beta(\Omega|\Omega') \to \alpha(\mathbf{v})$ and $\beta(\mathbf{v}|\mathbf{v}')$. Now $\alpha(\mathbf{v})$ is the initial probability distribution of velocities with angle Ω and speed v and $\beta(\mathbf{v}|\mathbf{v}')$ is the probability of scattering into angle Ω and speed v with incoming angle Ω' and speed v' prior to the collision,

$$\begin{aligned}\rho(\mathbf{x},t,\mathbf{v}) = {} & f(\mathbf{x},t,\mathbf{v})\alpha(\mathbf{v})\psi(t) + \int d^3\mathbf{x}'dt' f(\mathbf{x}-\mathbf{x}',t-t',\mathbf{v}) \\ & \times\psi(t-t')\int d^3\mathbf{v}'\beta(\mathbf{v}|\mathbf{v}')\rho(\mathbf{x}',t',\mathbf{v}'), \end{aligned} \tag{6}$$

where $f(\mathbf{x},t,\mathbf{v})$ is given by

$$f(\mathbf{x},t,\mathbf{v}) = \delta^{(N)}(\mathbf{x} - \mathbf{v}t) \tag{7}$$

for N dimensions. This is similar to the formulation in Ref. [16], where they derive the spectrum of the conditional density and correlation functions in one dimension for arbitrary scattering-time densities.

Now the scattering density

$$\rho(\mathbf{x}',t',\mathbf{v}') = N_s\sigma_{\text{tot}}(v')v'n(\mathbf{x}',t',\mathbf{v}'), \tag{8}$$

where N_s is the number of scatterers per unit volume, $\sigma_{\text{tot}}(v')$ is the total inelastic scattering cross section and $n(\mathbf{x}',t',\mathbf{v}')$ is

the density of particles with velocity v' at $(\mathbf{x}',t')$. The double differential cross section $\sigma(\mathbf{v}' \to \mathbf{v}) = \beta(\mathbf{v}|\mathbf{v}')\sigma_{\rm tot}(v')$.

For a system in thermal equilibrium:

$$n(\mathbf{x}',t',\mathbf{v}') = \alpha(\mathbf{v}')n(\mathbf{x}',t'). \tag{9}$$

For the common case $\sigma_{\rm tot}(v') \propto 1/v'$, we can write

$$\rho(\mathbf{x}',t',\mathbf{v}') = \alpha(\mathbf{v}')\rho(\mathbf{x}',t'), \tag{10}$$

where $\rho(x',t') = N_s\sigma_{\rm tot}(v')v'n(\mathbf{x}',t')$ is then independent of v'.

Thus the second term in Eq. (6) becomes

$$\begin{aligned}&\int d^3\mathbf{x}'dt'\, f(\mathbf{x}-\mathbf{x}',t-t',\mathbf{v})\psi(t-t')\\ &\quad\times\int d^3\mathbf{v}'\beta(\mathbf{v}|\mathbf{v}')\alpha(\mathbf{v}')\rho(\mathbf{x}',t')\\ &=\alpha(\mathbf{v})\int d^3\mathbf{x}'dt'\, f(\mathbf{x}-\mathbf{x}',t-t',\mathbf{v})\psi(t-t')\rho(\mathbf{x}',t'),\end{aligned} \tag{11}$$

making use of the property

$$\int d^3\mathbf{v}'\beta(\mathbf{v}|\mathbf{v}')\alpha(\mathbf{v}') = \alpha(\mathbf{v}), \tag{12}$$

which must be satisfied by any physically allowable kernel that produces a Maxwellian steady state. Thus our method is valid for a variety of experimentally relevant collision kernels such as the cusp kernels introduced in Ref. [17]. For a Markovian thermalization process $\beta(\mathbf{v}|\mathbf{v}') = \alpha(\mathbf{v})$ independent of $\mathbf{v}'$ and (11) follows directly from Eq, (6).

With this included our transport equations become

$$\begin{aligned}\rho(\mathbf{x},t,\mathbf{v}) = \alpha(\mathbf{v})f(\mathbf{x},t,\mathbf{v})\psi(t) + \alpha(\mathbf{v})\int d^3\mathbf{x}'dt'\\ \times f(\mathbf{x}-\mathbf{x}',t-t',\mathbf{v})\psi(t-t')\rho(\mathbf{x}',t'),\end{aligned} \tag{13}$$

$$\begin{aligned}p(\mathbf{x},t,\mathbf{v}) = \alpha(\mathbf{v})f(\mathbf{x},t,\mathbf{v})\Psi(t) + \alpha(\mathbf{v})\int d^3\mathbf{x}'dt'\\ \times f(\mathbf{x}-\mathbf{x}',t-t',\mathbf{v})\Psi(t-t')\rho(\mathbf{x}',t').\end{aligned} \tag{14}$$

The remarkable property of our model (13) and (14) is that it is independent of the form of the scattering kernel as as long as Eq. (12) is satisfied.

Since we are mainly interested in finding the velocity-averaged probability $p(\mathbf{q},s)$, we introduce the velocity-integrated quantities

$$p(\mathbf{x},t) = \int p(\mathbf{x},t,\mathbf{v})d^3\mathbf{v}, \tag{15}$$

$$\rho(\mathbf{x},t) = \int \rho(\mathbf{x},t,\mathbf{v})d^3\mathbf{v}. \tag{16}$$

The first term in Eq. (13) represents all of the particles that make their first scattering at $(\mathbf{x},t)$. The second term, a convolution of the f propagator and scattering density ρ represents particles that have scattered at $(\mathbf{x}',t')$ and traveled to $(\mathbf{x},t)$ where they make another collision. From here they can make another collision (13) or continue on the same path without scattering, but they contribute to the particle density at $(\mathbf{x},t)$ (14).

We take advantage of the convolution theorem of the Fourier–Laplace transform to solve for the spectrum, $p(\mathbf{q},s)$. Setting

$$\begin{aligned}g(\mathbf{x}-\mathbf{x}',t-t',\mathbf{v}) &= f(\mathbf{x}-\mathbf{x}',t-t',\mathbf{v})\psi(t-t'),\\ G(\mathbf{x}-\mathbf{x}',t-t',\mathbf{v}) &= f(\mathbf{x}-\mathbf{x}',t-t',\mathbf{v})\Psi(t-t'),\end{aligned} \tag{17}$$

we have from Eq. (13),

$$\rho(\mathbf{q},s,\mathbf{v}) = \alpha(\mathbf{v})g(\mathbf{q},s,\mathbf{v}) + \rho(\mathbf{q},s)\alpha(\mathbf{v})g(\mathbf{q},s,\mathbf{v}), \tag{18}$$

$$p(\mathbf{q},s,\mathbf{v}) = \alpha(\mathbf{v})G(\mathbf{q},s,\mathbf{v}) + \rho(\mathbf{q},s)\alpha(\mathbf{v})G(\mathbf{q},s,\mathbf{v}), \tag{19}$$

so that

$$p(\mathbf{q},s) = \frac{\int\alpha(\mathbf{v})G(\mathbf{q},s,\mathbf{v})d^3\mathbf{v}}{1-\int\alpha(\mathbf{v})g(\mathbf{q},s,\mathbf{v})d^3\mathbf{v}}. \tag{20}$$

For gas collisions that randomize velocity, after each collision the correct conditional probability density p is not a direct velocity average of the single velocity p but a function of the velocity average of the individual propagators of G and g.

The collision time and the probability of scattering $\psi(t)$ remain the same for all three dimensions,

$$\psi(t) = \frac{1}{\tau_c}e^{-\frac{1}{\tau_c}t}, \tag{21}$$

where $1/\tau_c$ is the rate of gas collisions. The probability of not making a scattering in time t is given by the integration over the scattering rate,

$$\Psi(t) = \int_t^\infty \psi(t)dt = e^{-\frac{t}{\tau_c}}. \tag{22}$$

We define

$$F_N(\mathbf{x},t) = \int \alpha_N(\mathbf{v})G_N(\mathbf{x},t,\mathbf{v})d^N\mathbf{v}, \tag{23}$$

where N represents the number of dimensions in the random walk. We now find the Fourier–Laplace transform of $F_N(\mathbf{x},t)$,

$$F_N(\mathbf{q},s) = \int_0^\infty dt\int\alpha_N(\mathbf{v})\delta^{(N)}(\mathbf{x}-\mathbf{v}t)e^{-\frac{t}{\tau_c}-i\mathbf{q}\cdot\mathbf{x}-st}d^N\mathbf{x}d^N\mathbf{v}. \tag{24}$$

We will use the Maxwellian velocity distribution:

$$\alpha_N(\mathbf{v}) = \prod_{i=1}^N\left(\frac{1}{2}\sqrt{\frac{2m}{\pi kT}}\right)e^{-\frac{m}{2kT}v_i^2}. \tag{25}$$

Substituting this into Eq. (24),

$$\begin{aligned}F_N(\mathbf{q},s) = \int_0^\infty dt\int\left[\prod_{i=1}^N\left(\frac{1}{2}\sqrt{\frac{2m}{\pi kT}}\right)e^{-\frac{m}{2kT}v_i^2}\right]\delta^{(N)}(\mathbf{x}-\mathbf{v}t)\\ \times e^{-\frac{t}{\tau_c}-i\mathbf{q}\cdot\mathbf{x}-st}d^N\mathbf{x}d^N\mathbf{v},\end{aligned} \tag{26}$$

and integrating over position gives

$$\begin{aligned}F_N(\mathbf{q},s) = \int_0^\infty dt e^{-(s+\frac{1}{\tau_c})t}\prod_{i=1}^N\left(\frac{1}{2}\sqrt{\frac{2m}{\pi kT}}\right)\\ \times\int e^{-\frac{m}{2kT}v_i^2-iq_iv_it}dv_i,\end{aligned} \tag{27}$$

and integration over v_i then gives

$$F_N(\mathbf{q},s) = \int_0^\infty dt e^{-(s+\frac{1}{\tau_c})t} \prod_{i=1}^{N} e^{-\frac{1}{2}\frac{kT}{m}t^2 q_i^2} \tag{28}$$

$$= \int_0^\infty dt e^{-(s+\frac{1}{\tau_c})t - \frac{1}{2}\frac{kT}{m}t^2 q^2}. \tag{29}$$

Finally, performing the Laplace transform we find

$$F_N(\mathbf{q},s) = \sqrt{\frac{\pi m}{2kTq^2}} e^{\frac{m}{2kT}\frac{(s+\frac{1}{\tau_c})^2}{q^2}} \operatorname{erfc}\left(\sqrt{\frac{m}{2kT}}\frac{s+\frac{1}{\tau_c}}{q}\right),$$

$$= \sqrt{\frac{\pi m}{2kTq^2}} e^{z^2} \operatorname{erfc}(z) \equiv F(q,z), \tag{30}$$

where

$$z(q,s) = \sqrt{\frac{m}{2kT}}\frac{1}{\tau_c}\frac{(1+s\tau_c)}{q}. \tag{31}$$

We have been working with the Laplace transform of various functions of time. This implies that these functions are causal, i.e., equal to zero for $t < 0$. If we make the replacement $s \to i\omega$ and take two times the real part of the resulting expression, the results will apply to the even $[f(-t) = f(t)]$ extension of the causal functions, in agreement with other authors (see, e.g., Ref. [6]). Unless specified, it should be assumed that a spectrum refers to the even extension. From now on we use

$$F(q,\omega) = F(q,z(q,s=i\omega)). \tag{32}$$

It is immediately seen that the result is independent of the number of dimensions, N. The dimensionality of the model only appears in q, where

$$q^2 = \sum_{i=1}^{N} q_i^2.$$

We note that q can never be negative; this is important to remember when integrating and/or summing over discrete values of q. However, q_i, a single component of $\mathbf{q}$, can be negative. The conditional density for any number of dimensions (20) can be written as

$$p(q,\omega) = 2\,\mathrm{Re}\left[\frac{F(q,\omega)}{1-\frac{1}{\tau_c}F(q,\omega)}\right]. \tag{33}$$

Thus, we observe agreement for the spectrum of the conditional probability given by the CTRWT for one, two, and three dimensions. Furthermore, there are no cross correlations between the different directions in Cartesian coordinates, therefore one can compute values of a higher-dimensional model from a lower-dimensional model, given that this model was projected from Cartesian coordinates. Assuming Cartesian coordinates and given no cross-correlation in the components of the functions being correlated we can compute a 3D result from three 1D results, or one 2D result and one 1D result. In the latter case, the 2D model can include functions with cross correlation.

Comparison with diffusion theory

To compare with diffusion theory, we define a length scale and ballistic collision time. Naturally, the ballistic time should scale linearly with the length and inversely with the thermal speed of the system, thus $\tau_b = L\sqrt{\frac{m}{kT}}$. For diffusion theory to be valid we must have $\tau_b/\tau_c \gg 1$ and $1 \gg \omega\tau_c$ so that z becomes very large for not-too-large q,

$$z \approx \sqrt{\frac{m}{2kT}}\frac{1}{\tau_c}\frac{1}{q} = \frac{1}{\sqrt{2}}\frac{\tau_b}{\tau_c}\frac{1}{qL_x} \gg 1.$$

For large z the asymptotic expansion for the complimentary error function can be used,

$$\operatorname{erfc}(z) \to \frac{e^{-z^2}}{\sqrt{\pi}z}\left(1-\frac{1}{2z^2}\right). \tag{34}$$

For now, we keep the full form of z prior to expansion of the error function and substitute Eq. (34) into Eq. (33),

$$p(q,s=i\omega) = 2\,\mathrm{Re}\left(\frac{(1+i\omega\tau_c)^2}{\frac{kT}{m}q^2\tau_c + i\omega(1+i\omega\tau_c)^2}\right). \tag{35}$$

We then take the diffusion limit ($\omega\tau_c \ll 1$) with the result

$$p(q,\omega) = 2\,\mathrm{Re}\left(\frac{1}{\frac{kT}{m}q^2\tau_c + i\omega}\right) = 2\,\mathrm{Re}\left(\frac{1}{(Dq^2)+i\omega}\right). \tag{36}$$

Since $D_N = \frac{\langle v_N^2\rangle}{N}\tau_c$ where N is the number of dimensions and $\langle v_N^2\rangle = N\frac{kT}{m}$, we have inserted the diffusion coefficient,

$$D = \tau_c\frac{kT}{m}. \tag{37}$$

Equation (36) is immediately seen to be the Fourier transform of the Green's function of the diffusion equation.

C. Vector velocity autocorrelation function in an infinite domain

The vector velocity autocorrelation function can be written as an integration over the vector components of velocity, analogous to the one-dimensional treatment in Ref. [16],

$$S_{\mathbf{vv}}(\mathbf{q},s) = \iint_{-\infty}^{\infty} \mathbf{v}\cdot\mathbf{v}_0 p_{\mathbf{vv}_0}(\mathbf{q},s)\alpha(\mathbf{v}_0)d^3\mathbf{v}_0 d^3\mathbf{v}. \tag{38}$$

where $p_{\mathbf{vv}_0}(\mathbf{q},s)$ is the [16] Fourier–Laplace transform of the conditional probability for a particle which has velocity $\mathbf{v}_o$ at $(\mathbf{x}=0,t=0)$ to have the velocity $\mathbf{v}$ at $(\mathbf{x},t)$ and satisfies,

$$p_{\mathbf{vv}_0}(\mathbf{q},s) = G_v(\mathbf{q},s)\delta(\mathbf{v}-\mathbf{v}_0) + \alpha(\mathbf{v})G_v(\mathbf{q},s)\rho_o(\mathbf{q},s), \tag{39}$$

where

$$\rho_o(\mathbf{q},s) = \frac{g(\mathbf{q},s,\mathbf{v}_o)}{1-\int\alpha(\mathbf{v})g(\mathbf{q},s,\mathbf{v})\mathbf{d}^3\mathbf{v}}, \tag{40}$$

is the Laplace–Fourier transform of the scattering density at $(\mathbf{x},t)$ of particles that started at $(\mathbf{x}=0,t=0)$ with velocity $\mathbf{v}_o$. Then,

$$p_{\mathbf{vv}_0}(\mathbf{q},s) = G_v(\mathbf{q},s)\delta(\mathbf{v}-\mathbf{v}_0) + \frac{\alpha(\mathbf{v})G_v(\mathbf{q},s)g(\mathbf{q},s,\mathbf{v}_o)}{1-\int\alpha(\mathbf{v})g(\mathbf{q},s,\mathbf{v})\mathbf{d}^3\mathbf{v}}, \tag{41}$$

and using as above $\frac{1}{\tau_c}G_{\mathbf{v}}(\mathbf{q},s) = g_{\mathbf{v}}(\mathbf{q},s)$ we have

$$S_{\mathbf{vv}}(\mathbf{q},s) = \int v^2 G_v(\mathbf{q},s)\alpha(\mathbf{v})d^3\mathbf{v} + \frac{\frac{1}{\tau_c}[\int \mathbf{v}\alpha(\mathbf{v})G_v(\mathbf{q},s)d^3\mathbf{v}]^2}{1-\frac{1}{\tau_c}\int \alpha(\mathbf{v})G_v(\mathbf{q},s)d^3\mathbf{v}}. \tag{42}$$

For simplicity we write this equation as

$$S_{\mathbf{vv}}(\mathbf{q},s) = H(\mathbf{q},s) + \frac{\frac{1}{\tau_c}\mathbf{K}(\mathbf{q},s)^2}{1-\frac{1}{\tau_c}L(\mathbf{q},s)}, \tag{43}$$

where

$$H(\mathbf{q},s) = \int v^2 G_v(\mathbf{q},s)\alpha(\mathbf{v})d^3\mathbf{v}, \tag{44}$$

$$L(\mathbf{q},s) = \int G_v(\mathbf{q},s)\alpha(\mathbf{v})d^3\mathbf{v}, \tag{45}$$

$$\mathbf{K}(\mathbf{q},s) = \int \mathbf{v}G_v(\mathbf{q},s)\alpha(\mathbf{v})d^3\mathbf{v}, \tag{46}$$

$$G(\mathbf{q},s) = \frac{1}{\left(s+\frac{1}{\tau_c}\right)+i\mathbf{q}\cdot\mathbf{v}}. \tag{47}$$

Carrying out all the integrations we find

$$S_{\mathbf{vv}}(q,s) = \frac{z+\sqrt{\pi}e^{z^2}(1-z^2)\mathrm{erfc}(z)}{\sqrt{\frac{m}{2kT}}q} - \frac{\lambda}{q^2}\frac{[\sqrt{\pi}ze^{z^2}\mathrm{erfc}(z)-1]^2}{1-\sqrt{\frac{\pi m}{2kT}}\frac{1}{\tau_c q}e^{z^2}\mathrm{erfc}(z)}. \tag{48}$$

This is the Fourier–Laplace transform for the velocity autocorrelation function of an unbounded continuous time random walk in 3D given a Maxwell velocity distribution, thermalizing gas collisions, and Poisson-distributed collision times.

To calculate the spectrum of the position-averaged velocity autocorrelation function we take the limit as $q \to 0$ ($z \gg 1$) and we use the asymptotic expansion of the erfc(z), equation (34), where we must take the expansion to the second term:

$$S_{\mathbf{vv}}(\omega) = \lim_{q\to 0}\left(\frac{z+(1-z^2)\frac{1}{z}\left(1-\frac{1}{2z^2}\right)}{\sqrt{\frac{m}{2kT}}q} - \frac{1}{\tau_c q^2}\frac{\left(\frac{1}{2z^2}\right)^2}{1-\sqrt{\frac{m}{2kT}}\frac{1}{\tau_c q}\frac{1}{z}\left(1-\frac{1}{2z^2}\right)}\right). \tag{49}$$

The second term in the sum does not contribute. This is expected from the derivation in Ref. [16] and signifies that the scattered trajectories do not contribute to the velocity autocorrelation function (VACF) because of cancellation when averaging over direction of the scattered particles. The first term can be simplified, and the limit taken, giving

$$S_{\mathbf{vv}}(\omega) = \lim_{q\to 0}\frac{\frac{3}{2z}-\frac{1}{2z^3}}{\sqrt{\frac{m}{2kT}}q}, \tag{50}$$

$$= \frac{3kT}{m}\frac{1}{\left(s+\frac{1}{\tau_c}\right)}, \tag{51}$$

which has an inverse Laplace transform,

$$R_{\mathbf{vv}}(t) = \frac{3kT}{m}e^{-\frac{t}{\tau_c}}. \tag{52}$$

This is the expected velocity autocorrelation function for an infinite domain. This particular result could have been found by finding the single component spectrum and multiplying by the number of dimensions, for this case the information in q contained in Eq. (48) is removed by the average over position ($q \to 0$).

III. STOCHASTIC MOTION IN BOUNDED DOMAINS

In Sec. II B we obtained a general expression for the propagator of our CTRWT model in an infinite domain. In this section we show how our result (33) may be used to construct the spectrum of the position and velocity autocorrelation functions in a bounded domain.

A. Spectrum of position and velocity autocorrelation functions in a bounded domain

We consider stochastic motion within a rectangular domain of the size $\{L_x, L_y, L_z\}$. By using the method of images [11], each reflection from a boundary is replaced by a particle coming from an image source, the original particle being considered as leaving the physical bounded region. So the probability of arriving at a given point, P(x,t) say, is given by the sum of probabilities of arriving from the original, physical source and all the image sources. As time increases more distant image sources come into play. Physically it is similar to standing between two perfect facing mirrors.

For each source point there is a set of image points, one each in a lattice of repetitions of the physical domain.

When we use this probability function to calculate averages of functions of position the probability P(x,t) has to be averaged over all possible starting positions in the physical cell and summed over all image points. This is equivalent to integrating the infinite domain probability function over all possible source points. For a more complete description, refer to Refs. [11,15,18,19].

The procedure can be clearly seen, for example, by considering the position coordinate as the function to be averaged. In this example, as we go along the coordinate (in the positive direction) in the physical cell, the coordinate increases. As we cross the boundary into the image cell the image coordinate reaches a maximum at the boundary and then decreases (negative slope). If we continue in this fashion the coordinate function will be a simple triangle wave, zero at the origin (asymmetric), with amplitude $L_x/2$ and period $2L_x$, the size of the physical cell being given by L_x.

Periodic functions can be represented in a Fourier series; for the triangle wave representing the position coordinate in the image cells centered at the origin we have

$$\widetilde{x}(x) = \sum_{n=\mathrm{odd}} -i^n \frac{2L_x}{\pi^2 n^2}e^{i\frac{\pi n}{Lx}x}. \tag{53}$$

The spectrum of the position correlation function can thus be written in terms of the periodic varying function $\widetilde{x}$:

$$S_{xx}(\omega) = \frac{1}{8\pi^3 L_x L_y L_z}\int_{-\mathbf{L}/2}^{\mathbf{L}/2} d^3\mathbf{x}_0 \int_{-\infty}^{\infty} d^3\mathbf{x} \times \int_{-\infty}^{\infty} d^3\mathbf{q}\widetilde{x}x_0 p(q,\omega)e^{-i\mathbf{q}\cdot(\mathbf{x}-\mathbf{x}_0)}, \quad (54)$$

where $p(q,\omega)$ is the conditional density found in Eq. (33). Integration over y and z gives $2\pi\delta(q_y)$ and $2\pi\delta(q_z)$, respectively. Due to the normalization in Eq. 54, subsequent integration over y_0 and z_0 will give unity. Integration over x gives

$$\sum_n -i^n \frac{2L_x}{\pi^2 n^2} 2\pi\delta\left(q_x - \frac{\pi n}{L_x}\right),$$

due to the definition of $\widetilde{x}$ in Eq. (53) where the sum is over n, where n are odd integers,

$$S_{xx}(\omega) = \frac{1}{L_x}\sum_{n=\text{odd}} -i^n \frac{2L_x}{\pi^2 n^2}\int_{-L/2}^{L/2} dx_0 x_0 \times p\left(q = |q_x| = \frac{\pi|n|}{L_x},\omega\right)e^{i\frac{\pi n}{L_x}x_0}. \quad (55)$$

Integrating over x_0 and taking the even extension of the causal function as above yields

$$S_{xx}(\omega) = \sum_{n=\text{odd}} \frac{4L_x^2}{\pi^4 n^4} p\left(|q_x| = \frac{\pi|n|}{L_x},\omega\right). \quad (56)$$

For the velocity autocorrelation function we have

$$S_{vv}(\omega) = \omega^2 \sum_{n=\text{odd}} \frac{4L_x^2}{\pi^4 n^4} p\left(\frac{\pi|n|}{L_x},\omega\right). \quad (57)$$

B. Long-time tails arise in diffusive motion in bounded domains.

The series expansion (56) for the spectrum of the position autocorrelation function is universal; it is valid for any mean-free path from the quasiballistic ($\xi = \tau_c/\tau_b \gg 1$) to the diffusive ($\xi \ll 1$) regime of motion. In this section we obtain closed-form expressions valid in the diffusive regime.

We start from Eq. (33):

$$p(q,\omega) = 2\text{Re}\left[\frac{\sqrt{\frac{m\pi}{2kT}}\frac{1}{q}e^{z^2}\text{erfc}(z)}{1-\sqrt{\frac{m\pi}{2kT}}\frac{1}{q\tau_c}e^{z^2}\text{erfc}(z)}\right] = 2\text{Re}\left[\tau_c\left(\frac{1}{1-\sqrt{\frac{m\pi}{2kT}}\frac{1}{q\tau_c}e^{z^2}\text{erfc}(z)}-1\right)\right], \quad (58)$$

where z is given by Eq. (31).

Assuming that the propagator is the even extension of the causal conditional probability $P(x,t)$, the spectrum of the position autocorrelation function in a finite system of size L_x reads [11] (56)

$$S_{xx}(\omega) = \frac{8{L_x}^2}{\pi^4}\sum_{n=1,3,\ldots}^{\infty}\frac{p(q_n,\omega)}{n^4}, \quad (59)$$

where

$$z_n = \sqrt{\frac{m}{2kT}}\frac{1+i\omega\tau_c}{q_n\tau_c}, \quad (60)$$

$$q_n = \frac{n\pi}{L_x}. \quad (61)$$

As shown in Appendix A 1, the result is

$$S_{xx}(\omega') = \frac{2\tau_c {L_x}^2\xi^2}{\omega'^2(1+\omega'^2)}(1-\Delta[\xi,\omega']), \quad (62)$$

where $\xi = \tau_c/\tau_b$, $\omega' = \omega\tau_c$, and

$$\Delta(\xi,\omega') = \frac{\sqrt{2}\xi}{(\omega')^{1/2}(1+\omega'^2)}\frac{\sin\left(\frac{\sqrt{\omega'}(1+\omega')}{\sqrt{2}\xi}\right)(1+2\omega'-\omega'^2)+\sinh\left(\frac{(1-\omega')\sqrt{\omega'}}{\sqrt{2}\xi}\right)(1-2\omega'-\omega'^2)}{\cos\left(\frac{\sqrt{\omega'}(1+\omega')}{\sqrt{2}\xi}\right)+\cosh\left(\frac{(-1+\omega')\sqrt{\omega'}}{\sqrt{2}\xi}\right)}. \quad (63)$$

Going back to original variables ω, τ_c, τ_b in the prefactor, noting that $(\frac{L_x}{\tau_b})^2 = kT/m$, and using $D = \frac{kT}{m}\tau_c$ (where D is the diffusion coefficient), we find

$$S_{xx}(\omega) = \frac{2\text{D}}{\omega^2[1+(\omega\tau_c)^2]}[1-\Delta(\xi,\omega\tau_c)]. \quad (64)$$

Note that our results (63) and (64) for the spectrum of the position correlation function is valid for any ω from 0 to ∞ as long as $\tau_c \ll \tau_b$, which is the condition for diffusive motion. Taking the limit $\omega \to 0$ we obtain

$$S_{xx}(0) = \frac{L_x^4}{60D} - \frac{1}{6}L_x^2\tau_c = \frac{L_x^4}{60D}(1-10\xi^2), \quad (65)$$

which is valid for the "nonadiabatic" regime of motion $\omega \ll 1/\tau_d$. Here, the first term is well known from "classical" diffusion theory [6]. The second term $\sim 10\xi^2$ is the next-order correction from our CTRWT model. When diffusion theory is valid, the correction is very small. We see that the prefactor in Eq. (64) does not involve any information on the system size, while the term $\Delta(\xi,\omega\tau_c)$ depends on the size of the system. Thus, the prefactor represents the spectrum for an infinite system $S_{xx}^{\text{inf}}(\omega)$ while the term $\Delta(\xi,\omega\tau_c)$ is a correction due to the finite size,

$$S_{xx}(\omega) = S_{xx}^{\text{inf}}(\omega)[1-\Delta(\xi,\omega\tau_c)], \quad (66)$$

$$S_{xx}^{\text{inf}}(\omega) = \frac{2\text{D}}{\omega^2(1+\omega^2{\tau_c}^2)}. \quad (67)$$

We may greatly simplify Eq. (63) by noting that, for large values of the argument $\sqrt{\omega\tau_c}(1-\omega\tau_c)/(\sqrt{2}\xi) \gg 1$ the hyperbolic functions dominate and Eq. (63) reduces to

$$\Delta(\xi,\omega\tau_c) \approx \text{sign}(1-\omega\tau_c)\frac{\sqrt{2}\xi(1-2\omega\tau_c-\omega^2{\tau_c}^2)}{(\omega\tau_c)^{1/2}(1+\omega^2{\tau_c}^2)}. \quad (68)$$

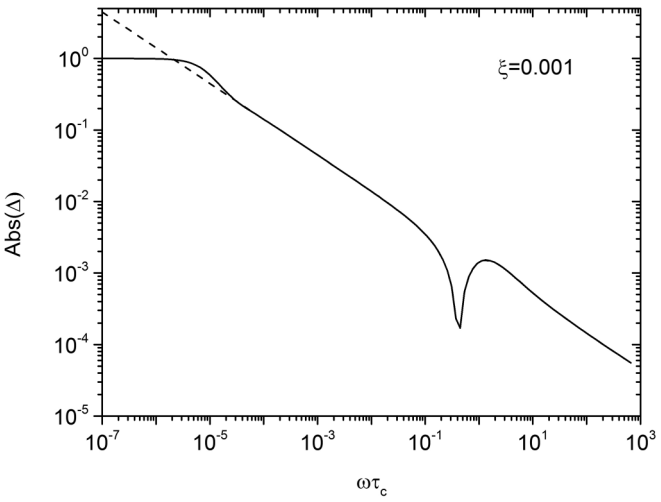

FIG. 1. Correction to the spectrum of position correlation function (63) due to the finite size of the system (solid line). Approximate correction (68) (dashed line). For $\omega\tau_c \ll 1$ the correction is negative; it has irregularities in the vicinity of $\omega\tau_c \sim 1$, where both functions abruptly change sign when $\omega\tau_c = 1$. However, the detailed behavior of the correction for $\omega\tau_c \gtrsim 1$ is of minor importance since its relative magnitude is small.

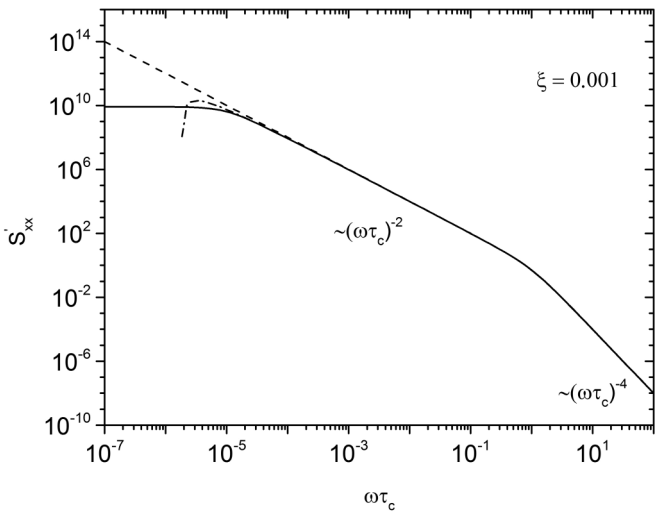

FIG. 2. Normalized position correlation spectrum $S_{xx}(\omega)/(2D{\tau_c}^2)$ calculated from Eq. (64) by using the exact finite-size correction (63) (solid line), the approximate correction (68) (dashed line), and for the infinite system (67) (dot-dashed line). Saturation of the spectrum for $\omega\tau_d < 1$ is a signature of the finite size.

In Fig. 1, we illustrate the frequency dependence of the finite-size corrections (63) (solid line) and (68) (dashed line).

For $\omega\tau_c \ll 1$, the condition $\sqrt{\omega\tau_c}(1-\omega\tau_c)/(\sqrt{2}\xi) \gg 1$ reduces to $\omega\tau_c \gg 2\xi^2$, or $\omega\tau_d \gg 2\pi^2$. This condition together with $\omega\tau_c \ll 1$ constitutes the classical conditions for the adiabatic regime of spin motion: $1/\tau_d \ll \omega \ll 1/\tau_c$. When these conditions are fulfilled,

$$\Delta(\xi,\omega\tau_c) \approx \frac{\sqrt{2}\xi}{(\omega\tau_c)^{1/2}}. \tag{69}$$

From analysis of Fig. 1 we conclude that the expression (68) indeed gives an excellent approximation of the exact result (63) for the adiabatic and "superadiabatic" regimes of spin motion. Figure 2 shows the normalized position correlation spectrum $S_{xx'}(\omega)/(D{\tau_c}^2)$ calculated from Eqs. (63) and (64) as well as by using approximation (68).

Spectrum of correlation function of single velocity component and long time memory in finite systems

In this section we show the existence of a long-time tail in the velocity autocorrelation function that arises only in the bounded domain. In free space it was shown in Eq. (52) that there is no long-time tail and that the velocity autocorrelation decays exponentially in time.

The spectrum of the correlation function of a single velocity component $S_{v_x v_x}(\omega)$ may be found from

$$S_{v_x v_x}(\omega) = \omega^2 S_{xx}(\omega), \tag{70}$$

which gives

$$S_{v_x v_x}(\omega) = S^{\rm inf}_{v_x v_x}(\omega)[1-\Delta(\xi,\omega\tau_c)], \tag{71}$$

$$S^{\rm inf}_{v_x v_x}(\omega) \approx \frac{2\rm D}{(1+\omega^2{\tau_c}^2)}, \tag{72}$$

where the finite-size correction $\Delta(\xi,\omega\tau_c)$ is the same as for the spectrum of the position correlation function.

Figure 3 shows the exact spectrum of the correlation function of a single velocity component given by Eqs. (63), (71), and (72) (solid line), as well as the spectrum obtained by using the approximation (68) (dashed line), and the spectrum for an infinite domain (72) (dot-dashed line).

By applying the inverse Fourier transform to Eq. (72) we recover the well-known result for the velocity correlation

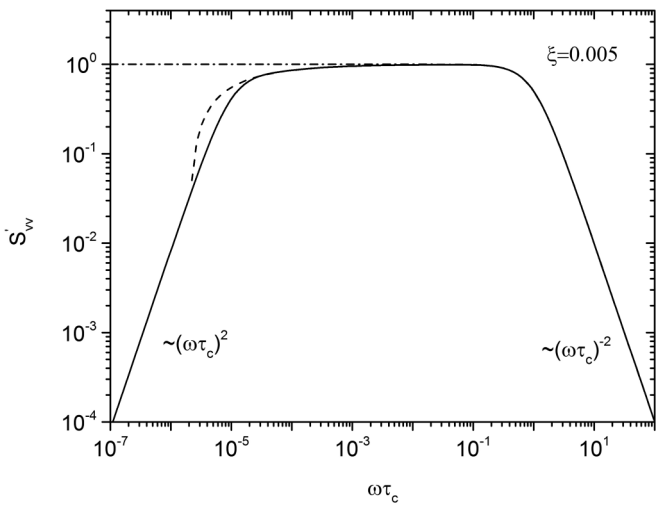

FIG. 3. Normalized spectrum of the correlation function for a single velocity component $S_{v_x v_x}/D$ calculated according to Eq. (71) by using the exact finite-size correction (63) (solid line), the approximate correction (68) (dashed line), and for the infinite system (72) (dot-dashed line). The low frequency cutoff for $\omega\tau_c \ll \xi^2$ is a signature of finite-size systems.

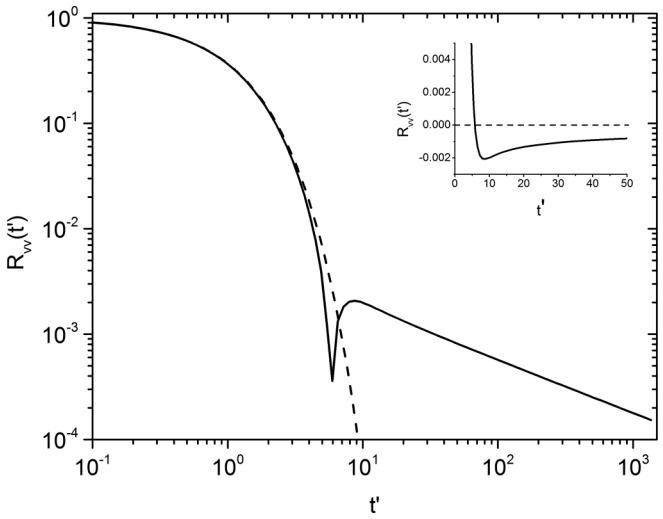

FIG. 4. Normalized velocity correlation function $R'_{vv}(t') = \frac{m}{kT} R_{vv}(t')$, where $t' = \frac{t}{\tau_c}$. Solid line shows the analytic result (74), valid for $t \ll \tau_d$. Dashed line shows the result for the infinite system (73). Negative spikes correspond to positions where functions charge sign. The inset shows the same function but on a linear scale.

function (52) for an infinite domain:

$$R^{\text{inf}}_{v_x v_x}(t) = \frac{kT}{m} e^{-|t|/\tau_c}. \tag{73}$$

The inverse Fourier transform for the exact result (63), (71), and (72) is unknown. However, the relatively simple form of Eq. (68) allows an inverse Fourier transformation. For $\tau_d \gg t \gg \tau_c$ we obtain

$$R_{v_x v_x}(t) \approx R^{\text{inf}}_{v_x v_x}(t) - \frac{2}{\sqrt{\pi}} \xi \frac{kT}{m} \left(\frac{t}{\tau_c}\right)^{-1/2}. \tag{74}$$

One can see that the finite-size correction has the form of a long-time tail $\sim(t/\tau_c)^{-1/2}$ with a relative magnitude of the order of $\xi = \tau_c/\tau_b$. Both solutions (73) and (74) are illustrated in Fig. 4.

For very short times $t \ll \tau_c$, all the results decay exponentially with a time constant τ_c. For longer times, only $R^{\text{inf}}_{v_x v_x}(t)$ decays exponentially. The velocity correlation function $R_{v_x v_x}(t)$ for a finite system has a very different behavior: for longer times it crosses the τ/τ_c axis from positive values to negative values (at the position where a spike is observed on the log-log plot) and, for even later times, it goes back toward the τ/τ_c axis being negative. It stays negative for very long times, until τ approaches τ_d, slowly decaying in magnitude according to a power law $\sim t^{-1/2}$. It may be shown (see Appendix A 1) that, for even longer times $\tau \gg \tau_d$, it again decays exponentially with time constant τ_d. This negative-long-time tail $\sim t^{-1/2}$ in the velocity correlation function is the same for 1D, 2D, and 3D systems and arises due to reflections from the system boundaries. This is in agreement with the one-dimensional treatment examined in Ref. [15]. This is in contrast to molecular dynamics where long-range hydrodynamic forces continuously act on the trajectories. These forces tend to produce cross correlation between motion in different directions; for example, vorticular motion. The cross correlation is examined in Ref. [20] (see also Ref. [21]). Including cross correlations of such kind leads to long-time tails $\propto t^{-d/2}$, where d represents the number of dimensions in the system. However, in systems of a relatively-low-density gas, the cross correlations resulting from hydrodynamic forces are suppressed, and our result completely describes the dynamics.

We can see the reason for the difference between our result and previous results showing a tail ($\sim t^{-d/2}$) by examining Ref. [20]. Equation (1) in that paper, while calculating the correlation function of a single velocity component, is a function of $k'^2 = \sum_{i=1}^{d} k_i'^2$. However, in calculating the position correlation function $\langle x_i(0)x_i(\tau)\rangle$ for each i, the dependence on the other components $j \neq i$ integrates out due to normalization of the conditional probability, so the correlation $\langle x_i(0)x_i(\tau)\rangle$ only depends on k_i. By using (A11) to get the correlation function of the individual velocity components v_i, we see that these each depend only on its particular k_i. The total velocity autocorrelation function $\langle \mathbf{v}(t) \cdot \mathbf{v}(t-\tau)\rangle$ is then the sum of d such terms. The result is then a sum of terms ($\sim t^{-1/2}$). Equation (1) in Ref. [20] contains products of functions of the different k_i and this results in the ($\sim t^{-d/2}$) behavior as shown in Eqs. (4), (16), and (18) of that work and implies correlations between the different directions of motion which do not occur in diffusion theory.

Another aspect of the long-time tail is a nonlinear behavior of the mean square displacement,

$$\begin{aligned}\langle x^2(t)\rangle &= 2\int_0^t (t-\tau)\langle v_x(0)v_x(\tau)\rangle d\tau \\ &= 2\frac{kT}{m}\int_0^t \left[e^{-t/\tau_c} - \frac{2}{\sqrt{\pi}}\xi\left(\frac{t}{\tau_c}\right)^{-1/2}\right](t-\tau)d\tau \end{aligned} \tag{75}$$

$$\approx 2Dt\left(1 - \frac{8}{3\sqrt{\pi}}\sqrt{\frac{t}{\tau_d}}\right). \tag{76}$$

Recall that our results (74) and, hence, (76) are valid for $\tau_c \ll t \ll \tau_d$. Again, we see that for not-too-long times $t \gg \tau_c$ the diffusion is a stationary Markovian process with

$$\langle x^2(t)\rangle = 2Dt \tag{77}$$

while, for longer times but still $t \ll \tau_d$, reflections from the boundaries will alter the linear dependence (77). While our correction is small, it is an indication of how the diffusion process eventually ends for $t \gg \tau_d$ in a homogeneous steady state with

$$\langle x^2(t \gg \tau_d)\rangle = \langle x^2\rangle. \tag{78}$$

As our results for the propagator have been shown to agree with diffusion theory in the limit $\xi = \frac{\tau_c}{\tau_b} \ll 1$, we expect that the long-time tail will also occur in the classical diffusion theory. We show this in an Appendix.

C. Spectrum of bounded domain position correlation function in ballistic or diffusive limits

1. Diffusive region

In the diffusion limit, the spectrum of the position autocorrelation function is observed to stratify into three regimes shown in Fig. 2:

(a) The nonadiabatic regime, defined by $\omega \ll \tau_d^{-1}$, with spectrum

$$S_{xx}(\omega) \approx S_{xx}(0) \approx \frac{1}{60}\frac{L_x^4}{D}. \tag{79}$$

(b) The adiabatic regime, defined by $\tau_d^{-1} \ll \omega \ll \tau_c^{-1}$, with spectrum

$$S_{xx}(\omega) \approx \frac{2\mathrm{D}}{\omega^2}. \tag{80}$$

(c) The superadiabatic regime, defined by $\tau_c^{-1} \ll \omega$, with spectrum

$$S_{xx}(\omega) \approx \frac{2\mathrm{D}}{\omega^4 \tau_c^2}. \tag{81}$$

Where the diffusion coefficient $D = \frac{k_B T}{m}\tau_c$ and the diffusion time $\tau_d = \frac{L^2}{\pi^2 D}$, the time constant for the lowest diffusion mode.

2. *Quasiballistic motion*

In this section we discuss some general properties of the spectrum of the position-position autocorrelation function (56) in the case of quasiballistic motion.

With decreasing pressure, the diffusion time decreases and the collision time τ_c increases. The motion is no longer diffusive when the time to cross the restricted volume approaches the collision time, $\tau_b = L/\sqrt{k_b T/m} \lesssim \tau_c$. This is considered to be the quasiballistic region and, in this region there exists no adiabatic regime, where $S_{xx}(\omega) \propto \omega^{-2}$, only two distinct regions are found.

Considering the limit $\xi = \tau_c/\tau_b \gg 1$ with the spectrum given by Eq. (56) leads us to distinguish three different regimes:

(a) The nonadiabatic regime or low-frequency region, $\omega \ll 1/\tau_c \ll 1/\tau_b$ and $|z_n| \ll 1$. In this regime we can replace $\exp({z_n}^2)\mathrm{erfc}(z_n)$ in Eqs. (30) and (33) by Eq. (34),

$$p(q_n,\omega) \approx 2\left(\frac{1}{1-\frac{1}{\sqrt{2\pi}n\xi}} - 1\right) \approx \frac{2\tau_c}{n\sqrt{2\pi}\xi},$$

with the spectrum of the position autocorrelation function given by Eq. (56),

$$S_{xx}(\omega) \approx \frac{16{L_x}^2}{\pi^4}\frac{1}{\sqrt{2\pi}\xi}\tau_c \sum_{n=1,3,\ldots}^{\infty}\frac{1}{n^5} = \frac{31 L_x^2 \tau_b \zeta(5)}{2\sqrt{2}\pi^{\frac{9}{2}}}, \tag{82}$$

where $\zeta(n)$ is the Riemann zeta function.

(b) The intermediate regime defined by $1/\tau_c \ll \omega \ll \sqrt{2}\pi/\tau_b$. In this regime z_n is mostly imaginary but still $|z_n| \ll 1$ and the low-z explanation is valid, leading to the same spectrum as above.

(c) The superadiabatic regime or high-frequency region, defined by $\sqrt{2}\pi/\tau_b \ll \omega$, with the spectrum found according to the large $|z| \gg 1$ expansion, Eq. (34), of the conditional density, Eq. (33),

$$S_{xx}(\omega) \approx \frac{2\mathrm{D}}{\omega^2(1+(\omega\tau_c)^2)} \approx \frac{2\mathrm{D}}{\omega^4 {\tau_c}^2},$$

$$S_{v_x v_x}(\omega) \approx \frac{2\mathrm{D}}{(\omega\tau_c)^2}.$$

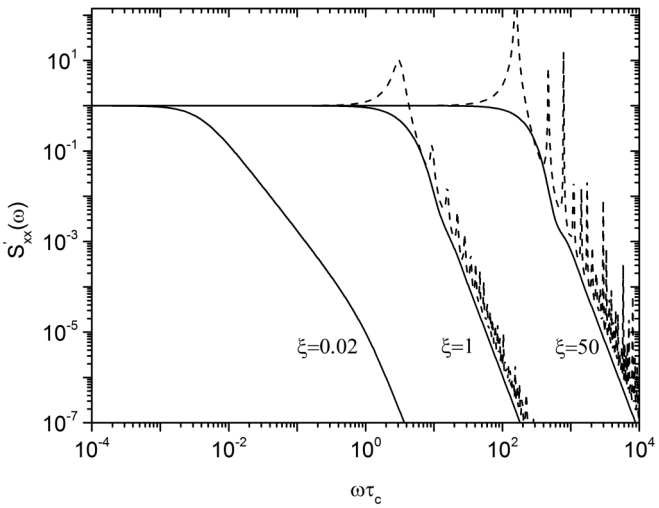

FIG. 5. The normalized spectrum of the position autocorrelation function $S'_{xx}(\omega) = \frac{S_{xx}(\omega)}{S_{xx}(0)}$, a comparison of the frozen picture with the thermalization picture in different regimes, diffusive ($\xi = 0.02$), intermediate ($\xi = 1$), and quasiballistic ($\xi = 50$). Solid lines represent predictions of our CTRWT model, dotted lines correspond to the CTRW in the frozen environment. For diffusive motion ($\xi = 0.02$) all models: CTRWT, CTRW in the frozen environment, and classical diffusion theory, give predictions which are indistinguishable in this plot.

Figure 5 shows spectra of the position correlation function for different regimes of motion from diffusive to quasiballistic; it is observed that scaling $\xi = \tau_c/\tau_b$ shifts the transition frequency for the quasiballistic nonadiabatic to superadiabatic regimes, when $\xi < 1$ the diffusion region is observed. It is interesting to compare the result for the spectrum of the position correlation function given by our CTRWT model, Eqs. (33) and (56), with the prediction [11] for the CTRW in a "frozen environment."

Figure 5 shows the evolution of the spectrum of position autocorrelation function from the diffusive ($\xi = .02$) to the quasiballistic ($\xi = 50$) regime of motion. Solid lines represent the predictions of our thermalizing CTRWT model, dotted lines corresponds to the model of CTRW in the frozen environment [11].

For quasiballistic motion in the frozen-environment model, collisions with the boundaries lead to the formation of resonances (for details see Ref. [11]). In this model the character of the structure of the resonances, as well as their width, depends on the parameter ξ and the number of dimensions in the the system. The higher is ξ the more narrow are the resonances. For the diffusive regime of motion ($\xi \ll 1$) the resonance structure is fully washed out and the prediction of all three models: our model of CTRWT, CTRW in the frozen environment, and classical diffusion theory [6] are indistinguishable.

The resonances in the ballistic region would be smoothed out by averaging the "frozen scatterer" spectrum over a Maxwell–Boltzmann velocity distribution; however, in the zero-frequency limit the velocity average of the spectrum diverges. Furthermore, velocity averaging the single velocity spectrum in the diffusion region gives results which depend on

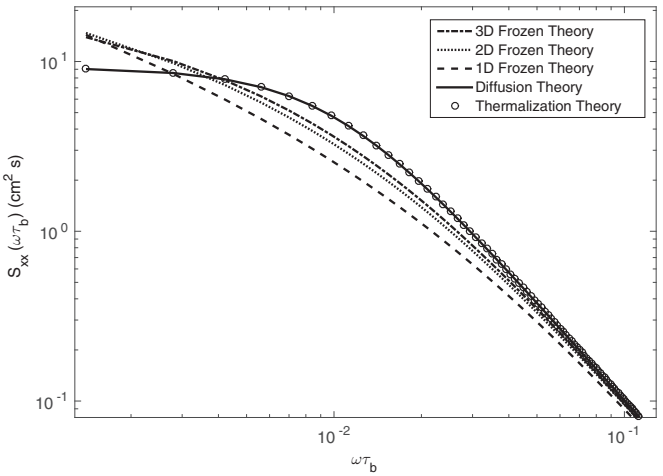

FIG. 6. The thermalization model compared to the frozen CTRW models, and diffusion theory for $T = 300$ mK, in the diffusion limit, $\omega\tau_c \ll 1$. Diffusion theory is accurate in this regime. We use the diffusion coefficient given by Ref. [22]. It is seen that the frozen CTRW models diverge from diffusion theory at low frequencies.

the number of dimensions, as shown in Fig. 6, in disagreement with the thermalization model presented here.

D. Application of bounded domain correlation functions

Another correlation function of particular physical interest is the position-velocity correlation function because it determines the frequency shift linear in the electric field of spins precessing in magnetic and electric fields. This is important in the search for electric dipole moments (EDMs), where the presence of an EDM results in frequency shifts which are also linear in the applied electric field [7,8]. With the use of integration by parts, the frequency shift can be written it terms of the imaginary component of the Fourier transform of the position autocorrelation function [3,23,24],

$$\delta\omega = -\omega\frac{\gamma^2 E}{c}\mathrm{Im}\left[\int_0^\infty e^{-i\omega\tau}\langle B_x(t)x(t+\tau) + B_y(t)y(t+\tau)\rangle d\tau\right] - \gamma^2\frac{E}{c}\langle B_x x + B_y y\rangle, \quad (83)$$

where E is the strength of the electric field applied in the z direction, and $B_{x,y}$ represents a perturbing magnetic field. $\langle\ldots\rangle$ represents an ensemble average. The frequency ω is determined by the applied holding field B_0, also in the z direction,

$$\omega = \gamma B_0. \quad (84)$$

The field B_x in Eq. (83) is a perturbation on the holding field B_0 manifest from the inevitable inhomogeneities of laboratory magnets. For accurate predictions of the relaxation and frequency shifts accounting for linear and quadratic terms are enough [25], any higher-order terms are negligible. Due to the correlation between field and position only asymmetric terms contribute, therefore only contributions from linear inhomogeneities are required for an accurate prediction. Therefore, we take

$$B_{x,y} \propto x, y,$$

and the phase shift due to the x component is proportional to the spectrum of the position autocorrelation function,

$$\delta\omega \propto \omega\mathrm{Im}[S_{xx}(\omega)] + \langle xx\rangle. \quad (85)$$

In this case $S_{xx}(\omega)$ is the spectrum obtained by using $p(q,s = i\omega)$, where $p(q,s)$ is the causal conditional density. A similar expression exists for the y component.

The thermalization model of the random walk presented in this work is now used to predict the phase shift of ^{3}He, Larmor precessing in a dilute solution in superfluid ^{4}He [26].

For a number-density ratio $^3\mathrm{He} : {}^4\mathrm{He} < 10^{-7}$, ^{3}He-^{3}He collisions can be ignored and collisions with the excitations in the superfluid dominate. The system is taken to be a rectangle of 10.2 by 40 by 7.6 cm. In superfluid helium, viscosity is absent [27] and the ^{3}He behaves as if it were in a vacuum with an increased mass $m^*_{^3\mathrm{He}} = 2.4m_{^3\mathrm{He}}$. The ^{3}He will thermalize by scattering on the excitations, phonons, and rotons in the superfluid. When the temperature of the superfluid is brought below 500 mK, phonons become the dominant excitation. In such a system the diffusion coefficient was measured [28,29] and the data were fit well by the equation

$$D = \frac{1.6}{T^7}. \quad (86)$$

We convert this to a collision time according to Eq. (37),

$$\tau_c = 1.6\frac{m}{kT^8}.$$

The predicted result is shown in Fig. 7 and as a function of temperature in Fig. 8 along with the result from [30]. The treatment of temperature is different in Ref. [30], where the single velocity random-walk result is averaged over a Maxwellian distribution of velocities. However an important prediction remains; a strong dependence on temperature of

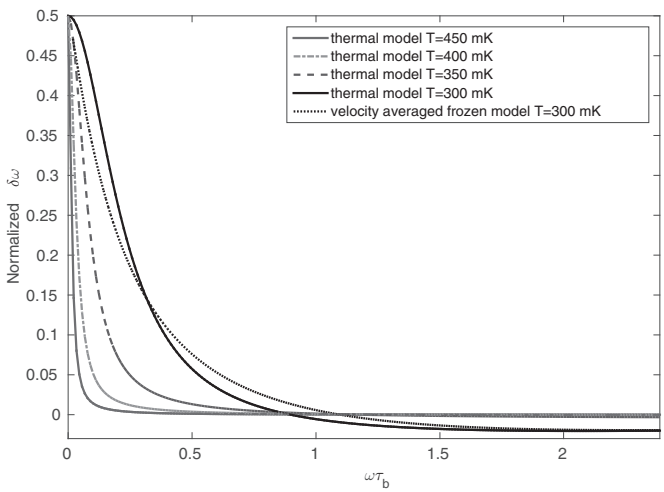

FIG. 7. The normalized spectrum of the linear-in-E phase shift bounded to a length of 40 cm for dilute ^{3}He dissolved in superfluid ^{4}He, with temperature as a parameter. All the solid curves are derived from the thermalization model, the dashed line is the velocity averaged frozen model [30].

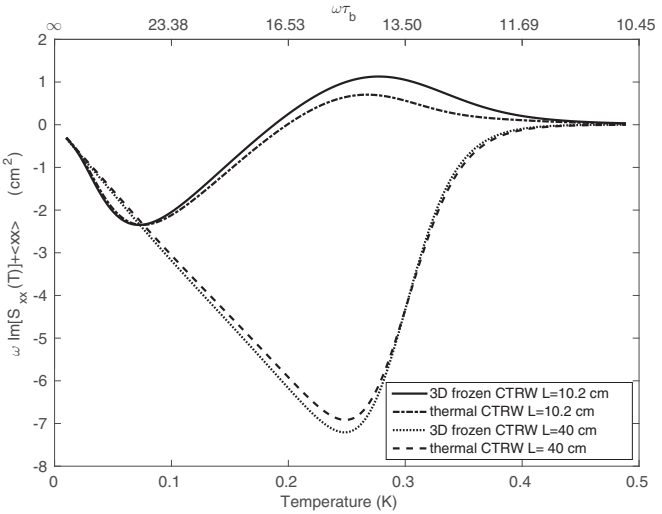

FIG. 8. The relative phase shift predicted from the thermalization model is compared with the single velocity models averaged over velocity. As the temperature decreases, and $\omega\tau_b(L = 40$ cm) increases, the models diverge.

the magnitude of the linear-in-E shift. Therefore varying the temperature is a tool to mitigate and study the effect.

Comparison of continuous time random walk with thermalization model with Monte Carlo simulations

A comparison with 1D, 2D, and 3D Monte Carlo simulations are done on 10^3 trajectories for 2×10^6 time steps. The trajectories are specific to ^{3}He at very low concentrations in superfluid ^{4}He at 400 mK, described in the previous Sec. III D. In this regime the mean-free path is determined

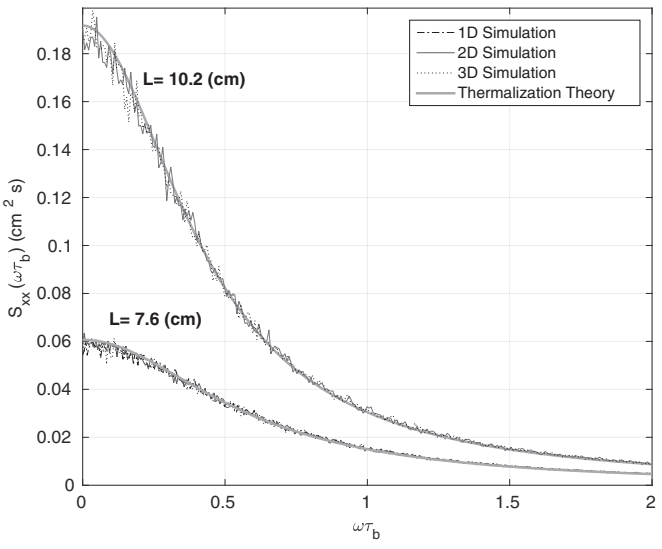

FIG. 9. The spectrum of the position autocorrelation function, a comparison of theory to 1D, 2D, and 3D simulations with thermalizing collisions for a temperature corresponding to 400 mK in the bulk. Good agreement is observed. Plotted are the correlation functions for one direction in which the cell length is either 7.6 or 10.2 cm. The third dimension in the 3D simulation is 40 cm; it is not shown.

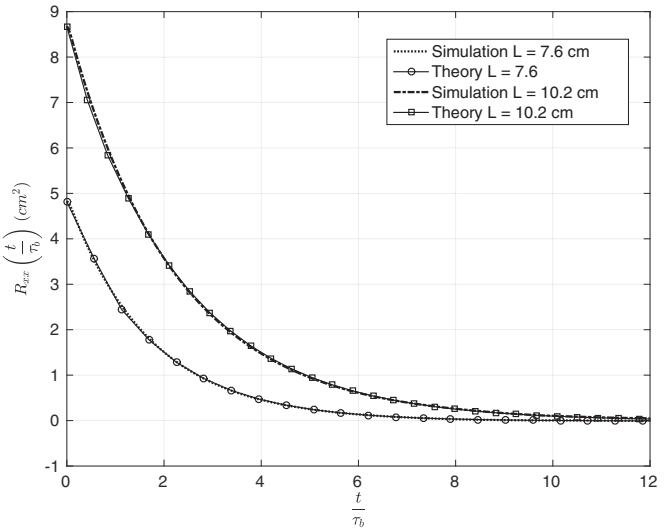

FIG. 10. The position autocorrelation function. The 3D simulation is compared to thermalization theory. Good agreement is observed.

by collisions with phonons in the superfluid. Upon a collision the new velocity was determined according to the isotropic 3D Maxwellian distribution. The trajectories are confined by specular wall collisions inside a rectangular volume 10.2 by 7.6 by 40 cm. The theoretical spectrum of the position autocorrelation function (56) is shown in Fig. 9 and compared with the results of the simulations. Figure 10 shows the position autocorrelation function as a function of time. The theoretical value of the position autocorrelation function is found from numerical inversion of the theoretical result for the spectrum except at $t = 0$. Due to the finite nature of the numerical inversion the $t = 0$ point is obtained by the mean squared average of position $\langle x(t)x(t)\rangle$.

IV. CONCLUSION

We have constructed a microscopic theory of the propagator (conditional probability density) for a persistent random walk where the particles undergo either Markovian stochastic scattering events or $1/v$ scattering satisfying detailed balance and maintaining thermal equilibrium in both cases. For a gas with a Maxwell–Boltzmann velocity distribution we obtain a relatively simple expression for the propagator. The result is independent of the number of dimensions considered, contrary to the frozen walk (i.e., a CTRW with fixed velocity) where the number of dimensions in the walk strongly effect the resonant structure of the correlation functions generated by the walk [11], and valid for all values of the scattering mean-free path from the quasiballistic to the diffusion regime of motion. We have shown directly that our results go over into the standard diffusion theory for short collision times (short mean-free paths). We have shown how the results can be applied to bounded regions by using the method of images and have given results for the position-position, position-velocity, and velocity-velocity correlation functions, all of which have direct applications in calculating frequency shifts and relaxation rates in NMR systems. One application is to the calculation of the NMR phase shift of ^{3}He in superfluid ^{4}He

in a magnetic and electric field. The results differ somewhat from the previous results obtained by averaging the frozen walk results over a Maxwell velocity distribution.

The method can be applied to inhomogeneous fields of any shape. We have discovered a universal long-time tail $\propto t^{-1/2}$ independent of dimensionality in bound systems. We emphasize that this long-time tail is expected only for bounded systems and is diminished with an increase in system size. While we show that this effect is predicted by the standard diffusion theory, in agreement with Ref. [15] who found a similar long-time tail by solving the one-dimensional Langevin equation, the independence of dimensionality does not seem to have been noticed before.

ACKNOWLEDGMENTS

We are grateful for fruitful discussion with Efim Katz on the long-time-tail problem and with Bart McGuyer concerning scattering kernels. We are grateful for the referee calling our attention to the external force problem in Ref. [13]. This work was supported in part by the US Department of Energy under Grant No. DE-FG02-97ER41042 and the US National Science Foundation under Grant No. 1506459.

APPENDIX A

1. Calculation of long-time tail from thermalization model

It is useful to introduce the dimensionless variables

$$\xi = \frac{\tau_c}{\tau_b} \quad \text{and} \quad \omega' = \omega\tau_c. \tag{A1}$$

In terms of the new variables, Eqs. (58) and (59) yield

$$z_n = \frac{1+i\omega'}{\sqrt{2}\xi\pi n}, \tag{A2}$$

$$S_{xx}(\omega') = \frac{16\tau_c {L_x}^2}{\pi^4}\left(-\frac{\pi^4}{96} + \sum_{n=1,3,\ldots}^{\infty}\frac{1}{n^4}\mathrm{Re}\right.$$
$$\left.\times\left\{1\Big/\left[1-(\sqrt{2\pi}n\xi)^{-1}e^{z_n^2}\mathrm{erfc}(z_n)\right]\right\}\right). \tag{A3}$$

The diffusive regime of motion is defined by $\xi \ll 1$,thus for not-too-high n, $z_n \gg 1$. Due to the strong cutoff by the prefactor n^{-4} in Eq. (A3) only a few lower-order terms are effective, which allows us to apply the asymptotic expansion for erfc(z) valid for $z \gg 1$ (see Ref. [31], 7.1.23),

$$e^{z^2}\mathrm{erfc}(z) \approx \frac{1}{\sqrt{\pi}z}\left(1-\frac{1}{2z^2}\right). \tag{A4}$$

By using Eq. (A4) we can write for the sum in Eq. (A3):

$$\sum_{n=1,3,\ldots}^{\infty}\frac{1}{n^4}\mathrm{Re}\left\{1\Big/\left[1-\frac{1}{\sqrt{2\pi}n\xi}\frac{1}{\sqrt{\pi}z_n}\left(1-\frac{1}{2{z_n}^2}\right)\right]\right\} \tag{A5}$$
$$= \mathrm{Re}\left[\sum_{n=1,3,\ldots}^{\infty}\frac{1}{n^4}\frac{(-i+\omega')^3}{in^2\pi^2\xi^2+\omega'(-i+\omega')^2}\right]$$
$$= \mathrm{Re}\left[\sum_{n=1,3,\ldots}^{\infty}\frac{1}{n^4}\frac{(-i+\omega')/\omega'}{1+\alpha^2n^2}\right], \tag{A6}$$

where

$$\alpha^2 = \frac{i\pi^2\xi^2}{\omega'(-i+\omega')^2}. \tag{A7}$$

The sum in Eq. (A6) converges,

$$S_n(\omega') = \sum_{n=1,3,\ldots}^{\infty}\frac{1}{n^4}\frac{(-i+\omega')/\omega'}{1-\alpha^2n^2}$$
$$= \frac{(-i+\omega')/\omega'}{96}\pi\left[\pi^3 - 12\pi\alpha^2 + 24\alpha^3\tanh\left(\frac{\pi}{2\alpha}\right)\right]. \tag{A8}$$

Replacing α by Eq. (A7),

$$\mathrm{Re}[S_n(\omega')] = \frac{\pi^4}{96} + \frac{\pi^4\xi^2}{8\omega'^2(1+\omega'^2)}$$
$$-\mathrm{Re}\left[\frac{(-1)^{3/4}\pi^4\xi^3\tanh\left(\frac{(-1)^{3/4}\sqrt{\omega'}(-i+\omega')}{2\xi}\right)}{4(\omega')^{5/2}(-i+\omega')^2}\right]. \tag{A9}$$

Expanding and taking the real part in Eq. (A9) we arrive at

$$\mathrm{Re}[S_n(\omega')] = \frac{\pi^4}{96} + \frac{\pi^4\xi^2}{8(\omega')^2(1+\omega'^2)}(1-\Delta[\xi,\omega']), \tag{A10}$$

with $\Delta[\xi,\omega']$ given by Eq. (63).

2. Calculation of long-time tail in ordinary diffusion theory

We start from the well-known relation

$$R_{v_xv_x}(t) = -\partial_t^2 R_{xx}(t). \tag{A11}$$

For a 3D diffusive motion in a rectangular domain the autocorrelation function of the displacement in each direction is given by a term of the form

$$R_{xx}(t) = \frac{8{L_x}^2}{\pi^4}\sum_{n=0}^{\infty}\frac{1}{(2n+1)^4}e^{-\frac{(2n+1)^2t}{\tau_d}}, \tag{A12}$$

where

$$\tau_d = \frac{{L_x}^2}{\pi^2 D}, \tag{A13}$$

is the time constant for the lowest diffusion mode. Expression (A12) is valid for not-too-short times, $t \gg \tau_c$ (τ_c is the mean time between particle collisions). Inserting Eq. (A12) into Eq. (A11) we find, in agreement with Eq. (62) in Ref. [15],

$$R_{v_xv_x}(t) = -\frac{8{L_x}^2}{\pi^4}\frac{1}{{\tau_d}^2}\sum_{n=0}^{\infty}e^{-\frac{(2n+1)^2t}{\tau_d}} = -\frac{4{L_x}^2}{\pi^4}\frac{1}{{\tau_d}^2}\vartheta_2\left(0,e^{-\frac{4t}{\tau_d}}\right), \tag{A14}$$

where $\vartheta_2(u,z)$ is Jacobi theta function. To investigate the short-time ($t \ll \tau_d$) behavior of the Jacobi theta function we expand it in a series and keep only lowest-order terms,

$$\vartheta_2\left(0,e^{-\frac{4t}{\tau_d}}\right) \approx \frac{\sqrt{\pi}\sqrt{\tau_d}}{2\sqrt{t}}. \tag{A15}$$

Inserting Eq. (A15) into Eq. (A14) we find

$$R_{v_x v_x}(t) = -\frac{4L^2}{\pi^4}\frac{1}{\tau_d^2}\frac{\sqrt{\pi}\sqrt{\tau_d}}{2\sqrt{t}} = -\frac{2}{\pi^{1/2}}\xi\frac{kT}{m}\left(\frac{t}{\tau_c}\right)^{-1/2}. \tag{A16}$$

For a longer times ($t \gg \tau_d$), $e^{-\frac{4t}{\tau_d}} \to 0$ and we may expand $\vartheta_2(0,z)$ for z $\to$ 0. Again keeping only lowest-order terms,

$$R_{v_x v_x}(t) = -\frac{8L^2}{\pi^4}\frac{1}{\tau_d^2}\exp\left[-\frac{t}{\tau_d}\right]. \tag{A17}$$

We see that Eq. (A16) is exactly the same as second term in Eq. (74). Hence, both diffusion theory and our CTRWT model predicts the existence of a long-time tail (A16) in the correlation function for each velocity component. This negative tail exists for $\tau_c \ll$ t $\ll \tau_d$, for even longer times the velocity correlation function decays exponentially with time constant τ_d; see Eq. (A17).

APPENDIX B: CARTESIAN PROJECTION FROM THREE DIMENSIONS, EQUIVALENCE FOR ARBITRARY VELOCITY DISTRIBUTIONS

The CTRW probability density defines how trajectories propagate and is typically used to calculate averages and correlation functions. In the case that the CTRW probability density function is isotropic, the velocity distribution associated with the CTRW is isotropic, and the function that is being averaged or correlated does not depend on one or more of the Cartesian coordinates, then the variable can be integrated away. The resulting function will only depend on one or two of the Cartesian coordinates. This is because cross correlation between the different coordinates in a Cartesian system is absent. The CTRWT can be expressed in terms of the spectrum of the $F(\mathbf{r},t)$, function as given by the equation

$$p(\mathbf{q},\omega) = \frac{F(\mathbf{q},\omega)}{1-\frac{1}{\tau_c}F(\mathbf{q},\omega)}, \tag{B1}$$

where

$$F_{ND}(\mathbf{x},t) = \int \alpha_{ND}(\mathbf{v})G_{ND}(\mathbf{x},t,\mathbf{v})d^N\mathbf{v}. \tag{B2}$$

We wish to verify that

$$F_{2D}(\mathbf{x},t) = \int F_{3D}(\mathbf{x},t)dz. \tag{B3}$$

During the remainder of this proof the 2D side is on the left, and the 3D side is on the right. Writing this in terms of the velocity-averaged G functions,

$$\int \alpha_{2D}(v)G_{2D}(\mathbf{x},t,\mathbf{v})d^2\mathbf{v} = \iint \alpha_{3D}(v)_{3D}G_{3D}(\mathbf{x},t,\mathbf{v})d^3\mathbf{v}dz, \tag{B4}$$

$$\int \alpha_{2D}(v)\delta^2(\mathbf{x}-\mathbf{v}t)e^{-\frac{t}{\tau_c}}d^2\mathbf{v} = \iint \alpha_{3D}(v)\delta^3(\mathbf{x}-\mathbf{v}t)e^{-\frac{t}{\tau_c}}d^3\mathbf{v}dz. \tag{B5}$$

In polar coordinates we can define the delta function

$$\delta^2(\mathbf{x}) = \frac{\delta(\rho)}{\rho}\delta(\phi), \tag{B6}$$

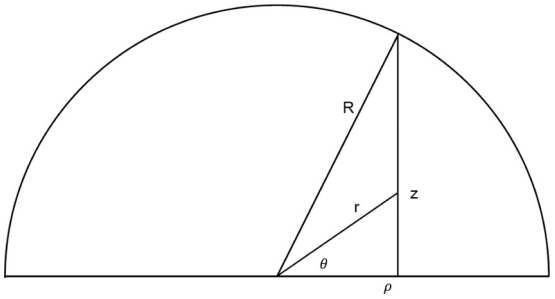

FIG. 11. Visualization of the projection from a higher dimension onto a lower dimension.

where $\rho = (x^2+y^2)^{1/2}$ and $\phi = \arctan(y/x)$. Similarly in spherical coordinates we have

$$\delta^3(\mathbf{x}) = \frac{\delta(r)}{r^2}\frac{\delta(\theta)}{\sin\theta}\delta(\phi), \tag{B7}$$

with $r = (x^2+y^2+z^2)^{1/2}$, $\theta = \arctan[(x^2+y^2)^{1/2}/z]$, and $\phi = \arctan(y/x)$.

Inserting these definitions into Eq. (B5) and writing the integration over polar and spherical coordinates we have

$$\iint \alpha_{2D}(v)\frac{\delta(\rho-vt)}{\rho}\delta(\phi-\phi_v)e^{-\frac{t}{\tau_c}}vdvd\phi_v \tag{B8}$$

$$= \iint \alpha_{3D}(v)\frac{\delta(r-vt)}{r^2}\frac{\delta(\theta-\theta_v)}{\sin\theta}\delta(\phi-\phi_v)e^{-\frac{t}{\tau_c}}v^2 \times \sin\theta_v dvd\theta_v d\phi_v dz. \tag{B9}$$

Integration over the angular coordinates in each gives

$$\int \alpha_{2D}(v_\rho)\frac{\delta(\rho-v_\rho t)}{\rho}e^{-\frac{t}{\tau_c}}v_\rho dv_\rho = \iint \alpha_{3D}(v)\frac{\delta(r-vt)}{r^2}e^{-\frac{t}{\tau_c}}v^2dvdz. \tag{B10}$$

We can continue if we assume that z can be determined from r and ρ according to Fig. 11 by

$$z = \sqrt{r^2-\rho^2}. \tag{B11}$$

Therefore, if we wish to integrate over z, the definition of a projection, we can change this to in integration over r by

$$dz = \frac{2rdr}{\sqrt{r^2-\rho^2}}. \tag{B12}$$

Inserting this into the right-hand side in equation (B10),

$$\int \alpha_{2D}(v_\rho)\frac{\delta(\rho-v_\rho t)}{\rho}e^{-\frac{t}{\tau_c}}v_\rho dv_\rho = \iint_\rho^\infty \alpha_{3D}(v)\frac{\delta(r-vt)}{r^2}e^{-\frac{t}{\tau_c}}v^2dv\frac{2rdr}{\sqrt{r^2-\rho^2}}, \tag{B13}$$

$$\int \alpha_{2D}(v_\rho)\frac{\delta(\rho-v_\rho t)}{\rho}e^{-\frac{t}{\tau_c}}v_\rho dv_\rho = \int_0^\infty \alpha_{3D}(v)e^{-\frac{t}{\tau_c}}\frac{2vdv}{t\sqrt{vt^2-\rho^2}}[1-\Theta(\rho-vt)]. \tag{B14}$$

$\Theta(\rho-vt)$ is the Heaviside step function, it is needed because $r \geqslant \rho$ and prevents the function from going imaginary.

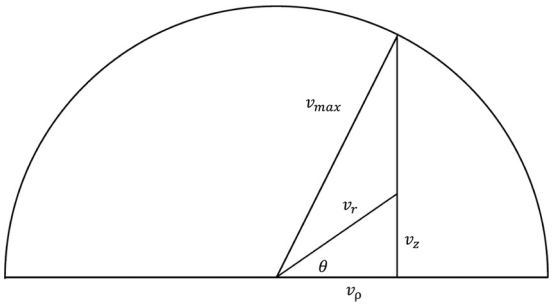

FIG. 12. Visualization of the projection from a higher dimension onto a lower dimension.

To continue we define a 2D velocity distribution, $\alpha(v_\rho)_{2D}$, as a projection from the 3D velocity distribution according to Fig. 12. Let us define the 2D velocity distribution as

$$\alpha_{2D}(v_\rho) = \int_{v_\rho}^{\infty} \frac{\alpha_{3D}(v)2vdv}{\sqrt{v^2 - v_\rho^2}}. \tag{B15}$$

Inserting this we have,

$$\iint_{v_\rho}^{\infty} \frac{\alpha_{3D}(v)2vdv}{\sqrt{v^2 - v_\rho^2}} \frac{\delta(\rho - v_\rho t)}{\rho} e^{-\frac{t}{\tau_c}} v_\rho dv_\rho$$
$$= \int_0^{\infty} \alpha_{3D}(v) e^{-\frac{t}{\tau_c}} \frac{2vdv}{t\sqrt{(vt)^2 - \rho^2}} [1 - \Theta(\rho - vt)]. \tag{B16}$$

We continue by scaling the delta function,

$$\iint_{v_\rho}^{\infty} \frac{\alpha_{3D}(v)2vdv}{\sqrt{v^2 - v_\rho^2}} \frac{\delta\left(v_\rho - \frac{\rho}{t}\right)}{t\rho} e^{-\frac{t}{\tau_c}} v_\rho dv_\rho$$
$$= \int_0^{\infty} \alpha_{3D}(v) e^{-\frac{t}{\tau_c}} \frac{2vdv}{t\sqrt{(vt)^2 - \rho^2}} [1 - \Theta(\rho - vt)]. \tag{B17}$$

Integrating over v_ρ we find

$$\int_{\frac{\rho}{t}}^{\infty} \frac{\alpha_{3D}(v)2vdv}{\sqrt{v^2 - \left(\frac{\rho}{t}\right)^2}} \frac{1}{t\rho} e^{-\frac{t}{\tau_c}} \frac{\rho}{t} \left[1 - \Theta\left(-\frac{\rho}{t}\right)\right]$$
$$= \int_0^{\infty} \alpha_{3D}(v) e^{-\frac{t}{\tau_c}} \frac{2vdv}{t\sqrt{(vt)^2 - \rho^2}} [1 - \Theta(\rho - vt)], \tag{B18}$$

$$\int_{\frac{\rho}{t}}^{\infty} \frac{\alpha_{3D}(v)2vdv}{t\sqrt{(vt)^2 - \rho^2}} e^{-\frac{t}{\tau_c}} \left[1 - \Theta\left(-\frac{\rho}{t}\right)\right]$$
$$= \int_0^{\infty} \alpha_{3D}(v) e^{-\frac{t}{\tau_c}} \frac{2vdv}{t\sqrt{(vt)^2 - \rho^2}} [1 - \Theta(\rho - vt)]. \tag{B19}$$

Again the Heaviside is there to keep the function real. In general we have $v > 0$ and $r \geqslant \rho$, so we can take the real part of the integral from zero to infinity,

$$\mathrm{Re}\left[\int_0^{\infty} \frac{\alpha_{3D}(v)2vdv}{t\sqrt{(vt)^2 - \rho^2}} e^{-\frac{t}{\tau_c}}\right]$$
$$= \mathrm{Re}\left[\int_0^{\infty} \frac{\alpha_{3D}(v)2vdv}{t\sqrt{(vt)^2 - \rho^2}} e^{-\frac{t}{\tau_c}}\right]. \tag{B20}$$

We verified that equation (B3) is valid. Therefore, with an isotropic velocity distribution we can find the results of the projected 3D random walk with the projected velocity distribution and the 2D random walk. We should point out that this projection is already satisfied by Maxwellian distributions, where we found that the conditional density is the same for 1D, 2D, and 3D.

The spectrum of a 3D CTRWT is a projection if the function in question does not depend on one or more of the Cartesian coordinates of the 3D system. Regardless of dimensions used in the model if a function does not depend on a particular Cartesian coordinate that coordinate can be integrated away. Consider the spectrum of an arbitrary function $h(\rho,\phi,z) = h(\rho,\phi)$ in cylindrical coordinates,

$$\int_{-\infty}^{\infty} h(\rho,\phi) e^{-i\mathbf{q}\cdot\mathbf{x}} d^3\mathbf{x} = H(q_\rho, q_\phi)\delta(q_z). \tag{B21}$$

We have $q_z = 0$ for all z. This is equivalent to integrating over the z direction and is the definition we used as a projection onto the x,y plane. Thus, when we solve for the Fourier transform we are automatically taking the projection onto the plane normal to the z direction. Therefore, isotropic velocity distributions in Cartesian coordinates allows the random walk in 1D or 2D to solve for the projections of the 3D random walk.

[1] N. Bloembergen, E. Purcell, and R. Pound, Relaxation effects in nuclear magnetic resonance absorption, Phys. Rev. **73**, 679 (1948).

[2] R. Golub, R. M. Rohm, and C. M. Swank, Reexamination of relaxation of spins due to a magnetic field gradient: Identity of the Redfield and Torrey theories, Phys. Rev. A **83**, 023402 (2011).

[3] G. Pignol, M. Guigue, A. Petukhov, and R. Golub, Frequency shifts and relaxation rates for spin-1/2 particles moving in electromagnetic fields, Phys. Rev. A **92**, 053407 (2015).

[4] A. Redfield, On the theory of relaxation processes, IBM J. Res. Dev. **1**, 19 (1957).

[5] C. P. Slichter, *Principles of Magnetic Resonance*, 3rd ed. (Springer, Berlin-Heidelberg, 1996).

[6] D. D. McGregor, Transverse relaxation of spin-polarized ^{3}He gas due to a magnetic field gradient, Phys. Rev. A **41**, 2631 (1990).

[7] J. M. Pendlebury, W. Heil, Y. Sobolev, P. G. Harris, J. D. Richardson, R. J. Baskin, D. D. Doyle, P. Geltenbort, K. Green, M. G. D. van der Grinten, P. S. Iaydjiev, S. N. Ivanov, D. J. R. May, and K. F. Smith, Geometric-phase-induced false electric dipole moment signals for particles in traps, Phys. Rev. A **70**, 032102 (2004).

[8] S. K. Lamoreaux and R. Golub, Detailed discussion of a linear electric field frequency shift induced in confined gases by a magnetic field gradient: Implications for neutron electric-dipole-moment experiments, Phys. Rev. A **71**, 032104 (2005).

[9] A. K. Petukhov, G. Pignol, D. Jullien, and K. H. Andersen, Polarized ^{3}He as a Probe for Short-Range Spin-Dependent Interactions, Phys. Rev. Lett. **105**, 170401 (2010).

[10] S. M. Clayton, Spin relaxation and linear-in-electric-field frequency shift in an arbitrary, time-independent magnetic field, J. Magn. Reson. **211**, 89 (2011).

[11] C. M. Swank, A. K. Petukhov, and R. Golub, Correlation functions for restricted Brownian motion from the ballistic through to the diffusive regimes, Phys. Lett. A **376**, 2319 (2012).

[12] J. Masoliver, J. M. Porra, and G. H. Weiss, Some two- and three-dimensional persistent random walks, Phys. A (Amsterdam, Neth.) **193**, 469 (1993).

[13] R. Burioni, G. Gradenigo, A. Sarracino, A. Vezzani, and A. Vulpiani, Rare events and scaling properties in field-induced anomalous dynamics, J. Stat. Mech. (2013) P09022.

[14] R. Burioni, G. Gradenigo, A. Sarracino, A. Vezzani, and A. Vulpiani, Scaling properties of field-induced superdiffusion in continuous time random walks, Commun. Theor. Phys. **62**, 514 (2014).

[15] I. Oppenheim and P. Mazur, Brownian motion in systems of finite size, Physica **30**, 1833 (1964).

[16] V. Zaburdaev, S. Denisov, and P. Hanggi, Space-Time Velocity Correlation Functions for Random Walks, Phys. Rev. Lett. **110**, 170604 (2013).

[17] B. H. McGuyer, R. Marsland, III, B. A. Olsen, and W. Happer, Cusp Kernels for Velocity-Changing Collisions, Phys. Rev. Lett. **108**, 183202 (2012).

[18] R. C. Wayne and R. M. Cotts, Nuclear-magnetic-resonance study of self-diffusion in a bounded medium, Phys. Rev. **151**, 264 (1966).

[19] J. C. Tarczon and W. P. Halperin, Interpretation of NMR diffusion measurements in uniform and nonuniform field profiles, Phys. Rev. B **32**, 2798 (1985).

[20] T. Keyes and B. Ladanyi, Long time tails in finite systems, J. Chem. Phys. **62**, 4787 (1975).

[21] R. F. A. Dib, F. Ould-Kaddour, and D. Levesque, Long-time behavior of the velocity autocorrelation function at low densities and near the critical point of simple fluids, Phys. Rev. E **74**, 011202 (2006).

[22] J. E. Opfer, K. Luszczynski, and R. E. Norberg, Diffusion coefficients and nuclear magnetic susceptibility of dilute ^{3}He, Phys. Rev. **172**, 192 (1968).

[23] G. Pignol and S. Roccia, Electric-dipole-moment searches: Reexamination of frequency shifts for particles in traps, Phys. Rev. A **84**, 042105 (2011).

[24] C. Swank, Ph.D. thesis, North Carolina State University, 2012.

[25] K. C. Hasson, G. D. Cates, K. Lerman, P. Bogorad, and W. Happer, Spin relaxation due to magnetic-field inhomogeneities: Quartic dependence and diffusion-constant measurements, Phys. Rev. A **41**, 3672 (1990).

[26] R. Golub and S. K. Lamoreaux, Neutron electric-dipole moment, ultracold neutrons and polarized ^{3}He, Phys. Rep. **237**, 1 (1994).

[27] John Wilks, *The Properties of Liquid and Solid Helium* (Oxford University Press, London, UK, 1967).

[28] S. K. Lamoreaux *et al.*, Measurement of the ^{3}He mass diffusion coefficient in superfluid ^{4}He over the 0.45–0.95 K temperature range, Europhys. Lett. **58**, 718 (2002).

[29] G. Baym, D. H. Beck, and C. J. Pethick, Transport in ultradilute solutions of ^{3}He in superfluid ^{4}He, Phys. Rev. B **92**, 024504 (2015).

[30] A. L. Barabanov, R. Golub, and S. K. Lamoreaux, Electric dipole moment searches: Effect of linear electric field frequency shifts induced in confined gases, Phys. Rev. A **74**, 052115 (2006).

[31] M. Abramowitz and I. Stegun, *Handbook of Mathematical Functions* (Dover Publications, Mineola, New York, 1964).